

A Straightforward Synthesis and Structure–Activity Relationship of Highly Efficient Initiators for Two-Photon Polymerization

Zhiquan Li,[†] Niklas Pucher,[†] Klaus Cicha,[‡] Jan Torgersen,[‡] Samuel C. Ligon,[†] Aliasghar Ajami,[§] Wolfgang Husinsky,[§] Arnulf Rosspeintner,^{||} Eric Vauthey,^{||} Sergej Naumov,[⊥] Tom Scherzer,[⊥] Jürgen Stampfl,[‡] and Robert Liska^{*,†}

[†]Institute of Applied Synthetic Chemistry, Vienna University of Technology, Getreidemarkt 9/163/MC, 1060 Vienna, Austria

[‡]Institute of Materials Science and Technology, Vienna University of Technology, Favoritenstrasse 9-11, 1040 Vienna, Austria

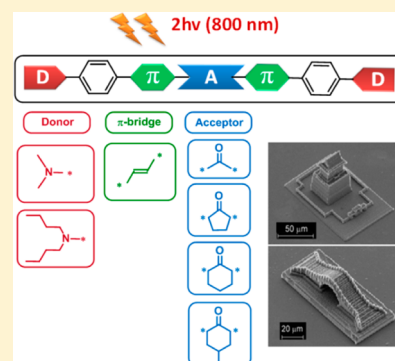
[§]Institute of Applied Physics, Vienna University of Technology, Wiedner Hauptstrasse 8, 1060 Vienna, Austria

^{||}Physical Chemistry Department, University of Geneva, Quai Ernest Ansermet 30, CH-1211 Geneva, Switzerland

[⊥]Leibniz Institute of Surface Modification (IOM), Permoserstrasse 15, D-04318 Leipzig, Germany

Supporting Information

ABSTRACT: The development of practical two-photon absorption photoinitiators (TPA PIs) has been slow due to their complicated syntheses often reliant on expensive catalysts. These shortcomings have been a critical obstruction for further advances in the promising field of two-photon-induced photopolymerization (TPIP) technology. This paper describes a series of linear and cyclic benzylidene ketone-based two-photon initiators containing double bonds and dialkylamino groups synthesized in one step via classical aldol condensation reactions. Systematic investigations of structure–activity relationships were conducted via quantum-chemical calculations and experimental tests. These results showed that the size of the central ring significantly affected the excited state energetics and emission quantum yields as well as the two-photon initiation efficiency. In the TPIP tests the 4-methylcyclohexanone-based initiator displayed much broader ideal processing windows than its counterparts with a central five-membered ring and previously described highly active TPA PIs. Surprisingly, a writing speed as high as 80 mm/s was obtained for the microfabrication of complex 3D structures employing acrylate-based formulations. These highly active TPA PIs also exhibit excellent thermal stability and remain inert to one-photon excitation. Straightforward synthesis combined with high TPA initiation efficiency makes these novel initiators promising candidates for commercialization.



INTRODUCTION

Two-photon induced photopolymerization (TPIP) has been intensively studied due to its unique nature allowing real 3D writing with very high resolution. The method has been exploited in various applications, such as photonic crystals,^{1,2} polymer-based optical waveguides on integrated circuit boards,³ high-density 3D optical data storage,^{4,5} and the like. The main advantage of TPIP is excellent spatial control due to the confinement of the photoactivated polymerization within the focal volume of the laser beams.⁶ Moreover, the use of a long wavelength excitation source (~ 800 nm) enables deeper penetration into the resin than UV light⁷ and reduces unwanted thermal or photochemical side reactions.

An efficient TPIP process requires active two-photon absorption photoinitiators (TPA PIs), which ensure high writing speeds, a low polymerization threshold, and therefore high-quality structures. One-photon radical PIs were usually used in the initial stages of TPIP research due to their commercial accessibility.^{8,9} However, as these PIs have rather low TPA cross sections (σ_{TPA}),¹⁰ high excitation power and long exposure time were required, which often resulted in damage to the polymeric structures. In the past decades, plenty

of TPA chromophores with large σ_{TPA} were synthesized, but only a limited number proved to be efficient TPA PIs.^{11–13} The main reason is that the rate of free radical photopolymerization is based not only on TPA but also on the quantum yields of radical generation and the initiating efficiency of the formed radicals. Thus, a large σ_{TPA} alone does not necessarily constitute a high photoinitiation efficiency.¹⁴

TPA PIs usually comprise dipolar or quadrupolar TPA chromophores containing planar π systems with long conjugation length and strong donors and/or acceptors.¹⁵ Unlike classical UV PIs, which have been successfully commercialized and widely used in protective and decorative coatings,¹⁶ TPA PIs are undergoing much slower development mainly limited to academic research. One important reason is that the formation of the desired planar π systems tends to require multistep synthesis and expensive catalysts. For example, double bonds are commonly introduced into existing π systems as bridges to extend the conjugation length. The

Received: August 23, 2012

Revised: December 12, 2012

Published: January 4, 2013

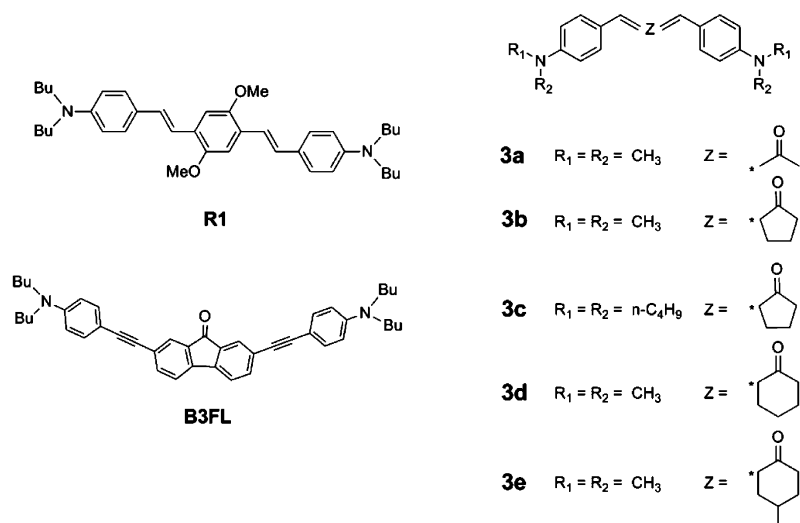


Figure 1. Structures of new TPA PIs and reference compounds.

desired products have mostly been realized by classical Wittig¹⁷ or Horner–Wadsworth–Emmons (HWE) reaction¹⁸ of non-commercial Wittig or HWE salts with corresponding aldehydes under strong alkaline conditions. A subsequent isomerization reaction with traces of iodine is generally required to convert undesired cis isomer to the desired trans product.¹⁹ Another method to make double-bond bridges is the Heck coupling reaction, a palladium-catalyzed reaction of aryl halides with terminal alkenes.²⁰ The main drawbacks of Heck coupling are the high price of palladium catalysts and difficulties associated with catalyst recycling.²¹ Although quite common, double-bond-containing TPA PIs tend to be less efficient than analogous triple-bond-based PIs due to the deactivation derived from potential photoinduced cis–trans isomerization.²² The Sonogashira coupling reaction is often employed to introduce alkyne groups into the backbone of PIs under ambient condition with high yields.^{23,24} Similar to the Heck reaction, such palladium-catalyzed coupling of aryl halides with terminal alkynes suffers from high costs. The needs for expensive catalysts or additional synthetic steps result in restrictively expensive TPA PIs, which have been obstructive for the development of TPIP technology. Therefore, it is crucial to develop simple and economical synthetic routes to provide efficient TPA PIs.

Benzylidene cyclopentanone dyes have been widely employed as highly efficient triplet photosensitizers in the UV photopolymerization industry.²⁵ Recently, Wu's group reported the synthesis of a series of benzylidene cyclopentanone dyes and successfully applied them as TPA PIs in TPIP.^{26,27} The D- π -A- π -D core structures of benzylidene ketone dyes could be simply built in one step via a classical aldol condensation reaction. Although a few studies on the structure–property relationship of benzylidene ketone dyes have been carried out by changing the terminal donor groups^{26,28} and extending the conjugation length,²⁹ the effects of locking the central ketone within different size rings have not been systematically studied up to now. In fact, the size of the central ring significantly affects the photochemical and photophysical characteristics, such as fluorescence emission.³⁰ Central cyclohexanone compounds possess much weaker fluorescence than their cyclopentanone counterparts.³¹ To be effective as a TPA initiator, if the triplet of the initiator is involved, low

fluorescence quantum yields are preferred as this leads to a higher population of the active, i.e. triplet, state for initiating the polymerization.³² On the other hand, testing the effects of ring size on photochemical properties is a flexible and practical method because various cycloketones are commercially available at relatively low costs. Combining the synthetic merits of the aldol condensation reaction with a systematic study on the effect of the central ring on TPIP performance should elucidate relevant routes providing highly efficient TPA PIs in a simple and economic manner.

In this article several benzylidene ketones with different central rings were prepared, and their photochemical behaviors in TPIP were investigated. For comparison, the highly efficient TPA PIs **R1**, well-known from the literature,¹² and **B3FL** (Figure 1), recently reported by our group,³³ were also tested. Investigation on the photophysical properties of the initiators was conducted via UV–vis absorption and emission as well as z-scan measurements. Quantum-chemical calculations were carried out to study the structure–property relationship, and the calculated results were compared with the experimental ones. Finally, TPIP structuring tests at different laser intensities and feed rates were performed to evaluate the TPA initiation efficiency of each initiator.

EXPERIMENTAL SECTION

Materials. All reagents for synthesis were purchased from Sigma-Aldrich, Fluka, and ABCR and were used without further purification unless otherwise noted. The solvents were dried and purified by standard laboratory methods. Column chromatography was performed with conventional techniques on VWR silica gel 60 (0.040–0.063 mm particle size). Aluminum-backed silica gel plates were used for TLC analyses.

Synthesis. General Procedure for Aldol Condensation Reaction. 20 mmol of benzaldehyde compound and 10 mmol of freshly distilled cycloketone compound were dissolved in 30 mL of ethanol. To this solution 10 mmol of sodium hydroxide dissolved in 3 mL of deionized water was added dropwise. The reaction was stirred at room temperature until the benzaldehyde compound was completely consumed (TLC analysis). The solution was diluted with 200 mL of chloroform and washed with a saturated NH_4Cl solution (3×75 mL) until the aqueous phase was neutral. The combined organic phases were dried over sodium sulfate and filtered, and the solvents were evaporated. The crude product was purified by recrystallization from ethanol or by column chromatography.

(1*E*,4*E*)-1,5-Bis[4-(*N,N*-dimethylamino)phenyl]-1,4-pentadien-3-one (**3a**). Purification by column chromatography (CHCl₃:EtOAc = 30:1) yielded the product of **3a** as orange crystals with a yield of 79%; mp 193–195 °C (lit.:³⁴ 196 °C). ¹H NMR (200 MHz, CDCl₃): δ (ppm) = 7.69 (d, *J* = 15.72 Hz, 2H), 7.51 (d, *J* = 8.86 Hz, 4H), 6.89 (d, *J* = 15.72 Hz, 2H), 6.68 (d, *J* = 8.86 Hz, 4H), 3.02 (s, 12H). ¹³C NMR (50 MHz, CDCl₃): δ (ppm) = 188.99, 151.86, 143.04, 130.19, 123.00, 121.41, 111.98, 40.25.

(2*E*,5*E*)-2,5-Bis(4-(dimethylamino)benzylidene)cyclopentanone (**3b**). Purification by column chromatography (CHCl₃:EtOAc = 30:1) yielded the product of **3b** as orange crystals with a yield of 92%; mp >300 °C decomp. (lit.:³⁵ >320 °C). ¹H NMR (200 MHz, CDCl₃): δ (ppm) = 7.53 (d, *J* = 8.60 Hz, 4H), 7.52 (s, 2H), 6.77 (d, *J* = 8.62 Hz, 4H), 3.05 (s, 4H), 3.04 (s, 12H). ¹³C NMR: insoluble in various solvents.

(2*E*,5*E*)-2,5-Bis(4-(dibutylamino)benzylidene)cyclopentanone (**3c**). Purification by column chromatography (chloroform) followed by washing with cold PE yielded the product of **3c** as red crystals with a yield of 57%; mp 133–135 °C. ¹H NMR (200 MHz, CDCl₃): δ (ppm) = 7.51 (s, 2H), 7.50 (d, *J* = 8.46 Hz, 4H), 6.66 (d, *J* = 8.87 Hz, 4H), 3.32 (t, *J* = 7.46 Hz, 8H), 3.05 (s, 4H), 1.72–1.48 (m, 8H), 1.48–1.24 (m, 8H), 0.97 (t, *J* = 7.19 Hz, 12H). ¹³C NMR (50 MHz, CDCl₃): δ (ppm) = 196.03, 148.76, 133.51, 133.09, 132.86, 123.41, 111.43, 50.82, 29.53, 26.77, 20.40, 14.07. Anal. Calcd for C₃₅H₅₀N₂O: C, 81.66; H, 9.79; N, 5.44. Found: C, 81.29; H, 9.80; N, 5.53.

(2*E*,6*E*)-2,6-Bis(4-(dimethylamino)benzylidene)cyclohexanone (**3d**). Purification by recrystallization from ethanol yielded the product of **3d** as orange crystals with a yield of 45%; mp 245–247 °C (lit.:³⁶ 247–248 °C). ¹H NMR (200 MHz, CDCl₃): δ (ppm) = 7.77 (s, 2 H), 7.46 (d, *J* = 8.8 Hz, 4 H), 6.72 (d, *J* = 8.8 Hz, 4 H), 3.03 (s, 12 H), 2.95 (m, 4 H), 1.82 (m, 2 H). ¹³C NMR (50 MHz, CDCl₃): δ (ppm) = 190.1, 150.3, 137.0, 132.4, 124.3, 111.6, 40.2, 28.7, 23.2.

(2*E*,6*E*)-2,6-Bis(4-(dimethylamino)benzylidene)-4-methylcyclohexanone (**3e**). Purification by recrystallization from ethanol yielded the product of **3e** as orange crystals with a yield of 40%; mp 209–210 °C (lit.:³⁷ 212–214 °C). ¹H NMR (200 MHz, CDCl₃): δ (ppm) = 7.77 (s, 2 H), 7.46 (d, *J* = 8.8 Hz, 4 H), 6.77 (d, *J* = 8.8 Hz, 4 H), 3.14–3.05 (m, 2H), 3.04 (s, 12 H), 2.62–2.41 (m, 2 H), 1.93–1.85 (m, 1H), 1.11 (d, *J* = 6.7 Hz, 3 H). ¹³C NMR (50 MHz, CDCl₃): δ (ppm) = 189.7, 149.9, 137.4, 132.3, 131.6, 124.3, 111.7, 40.2, 36.8, 29.5, 22.0.

Characterization. ¹H NMR (200 MHz) and ¹³C NMR (50 MHz) spectra were measured with a Bruker ACE 200 FT-NMR spectrometer. The chemical shift (s = singlet, bs = broad singlet, d = doublet, t = triplet, m = multiplet) is stated in ppm using the nondeuterated solvent as internal standard. Solvents with a grade of deuteration of at least 99.5% were used. Melting points were measured on a Zeiss axiscope microscope with a Leitz heating block and remained uncorrected. GC-MS runs were performed on a Thermo Scientific DSQ II using a BGB 5 column (*l* = 30 m, *d* = 0.32 mm, 1.0 μm film; achiral). Elemental microanalysis was carried out with an EA 1108 CHNS-O analyzer from Carlo Erba at the microanalytical laboratory of the Institute for Physical Chemistry at the University of Vienna.

Calculations. In order to learn more about TPIP, quantum-chemical calculations were carried out on the structures of all new TPA PIs and the reference compounds **R1** and **B3FL** using density functional theory (DFT) B3LYP^{38–40} hybrid functional. The molecular geometries and frequency analysis of all studied molecules were calculated at the B3LYP/6-31G(d) level of theory (Jaguar version 7.8, release 111 program).⁴¹

The UV–vis spectra were calculated in vacuum and different solvents with the time-dependent (TD)⁴² DFT method at the B3LYP/6-31+G(d) level of theory. The energies of the lowest triplet states (T₁) were calculated both as the difference of zero point (ZPE) corrected electronic energies Δ*E*₀ (*E*₀ = *E* + ZPE) between the most stable structures of the singlet (S₀) and optimized triplet states and at TD B3LYP/6-31G(d) level as implemented in the Gaussian 03 program.⁴³

Solvent effect (cyclohexane, acetonitrile, and water in the present case) on the molecular structure and the energies of excited states was tested on the **3a** structure using Jaguar's Poisson–Boltzmann solver (PBF).⁴⁴ Additionally, UV–vis spectra in different solvents were calculated using self-consistent isodensity polarizable continuum (SCI-PCM) model⁴⁵ (Gaussian 03). A maximal bond change due to the solvent effect of water was observed for the carbonyl bond (0.016 Å). The calculated excitation energy in water shows a red shift for S₁ (0.25 eV). Molecular orbitals (MOs) and UV–vis spectra were visualized in graphical form with the help of the ChemBio3D Ultra program.⁴⁶

Photophysics. Absorption spectra were recorded on a Cary 50 absorption spectrometer. Emission spectra and excitation anisotropy spectra were obtained on a Cary Eclipse at a controlled temperature of 20 °C. Absorption and emission spectra were baseline corrected using the pure solvent. Absorption spectra were obtained on samples with a maximal absorbance of ~1, while the maximal absorbance for the emission spectra did not exceed 0.15. The emission spectra were corrected for the wavelength sensitivity of the apparatus using a set of fluorescence standards.⁴⁷ Emission quantum yields were obtained using Coumarin 314 in ethanol as a secondary emission standard (Φ_f = 0.86)⁴⁸ and using the equation⁴⁹

$$\Phi_s = \frac{\int I_s(\lambda) d\lambda}{\int I_r(\lambda) d\lambda} \frac{1 - 10^{-A_r}}{1 - 10^{-A_s}} \frac{n_r^2}{n_s^2} \Phi_r \quad (1)$$

where Φ_x is the fluorescence quantum yield of the sample (s) and reference (r) and I_x(λ) denotes the corresponding fluorescence spectra. A_x is the absorbance at the excitation wavelength, and n_x denotes the refractive index of the sample (s) and reference (r) solution.

Fluorescence lifetimes were measured on a home-built time-correlated single photon counting device using either a 400 or 470 nm laser diode (PicoQuant) as excitation source. The time resolution, as judged from the full width at half-maximum of the instrument response function, was ~200 ps.

Cyclohexane (Sigma-Aldrich, puriss. p.a.), *n*-butyl ether (Acros, 99+%), *n*-propyl acetate (Alfa Aesar, 99%), dichloromethane (Sigma-Aldrich, puriss. p.a.), ethanol (Fluka, puriss. p.a.), and acetonitrile (Roth, >99.9%) were used as received.

Z-Scan Analysis. A Ti:sapphire laser system (90 fs pulse duration, 1 kHz repetition rate) was used for the open aperture z-scan analysis. A detailed description of the setup and the fitting equations used can be found elsewhere.³³ Rhodamine B in methanol was used as reference standard to verify the reliability of the experimental setup. All PIs were prepared as 1.0 × 10⁻² M solutions in spectroscopic grade chloroform. The excited volume is refreshed approximately every 100 pulses, which approximately corresponds to 10 times for each z-position, which was found to be sufficient. The measurements were carried out at different pulse energies in the range 15–240 nJ. At higher energies a signal of the pure solvent appears and the solvent will contribute to the effective nonlinear absorption and even thermal effects are more likely to influence the measurement. Care had to be taken to collect the whole transmitted laser energy using a big diameter and short focal length lens. Additionally, a proper Gaussian beam profile in time and space is essential for the analysis.

TPIP Structuring Tests. Laser Device. For the direct laser writing of 3D structures, a Ti:sapphire laser providing NIR pulses at 780 nm with a pulse duration of 100 fs is used. The system operates at a repetition rate of 80 MHz. Direct laser writing with this system is usually carried out at a laser power below 10 mW (measured after passing the microscope objective). The laser is focused by a 100× oil immersion microscope objective (NA = 1.4), and the sample is mounted on a high-precision piezoelectric XYZ scanning stage with 200 nm positioning accuracy.

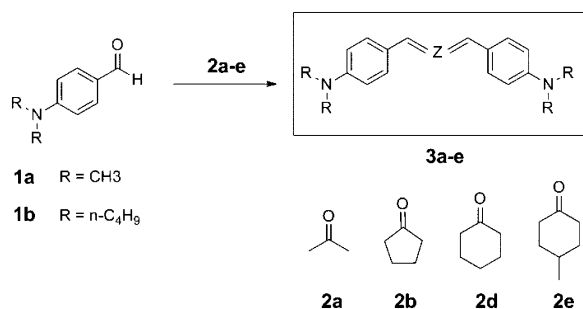
General Procedure. For all samples the same fabrication process was implemented: The optical material was drop-cast onto a glass substrate. Subsequently, the samples were exposed to the laser beam, and the focus was scanned across the photosensitive material, which leads to an embedded 3D structure inside the material volume. After laser writing, the unexposed material was removed by development of

the structure in ethanol (rinsing). The resulting structures, particularly their structural dimensions, integrity, and surface quality, were studied by means of scanning electron microscopy (SEM).

RESULTS AND DISCUSSION

Synthesis. All TPA PIs were synthesized via classical aldol condensation reactions between *N*-substituted benzaldehydes and corresponding ketones, both of which are commercially available and inexpensive. Aldol condensation is an effective method for carbon–carbon double bond formation between various carbonyl compounds. The reaction can be catalyzed with strong bases or acids⁵⁰ and complexes of metal(II) ions.⁵¹ For ease of preparation and reduced costs, sodium hydroxide was used as catalyst for the condensation.

Scheme 1. Reaction Scheme for the Synthesis of the TPA PIs



At room temperature, 1 equiv of the corresponding ketone was deprotonated at the α -position within a saturated sodium hydroxide solution. The formed enol interacts with 2 equiv of the aldehyde and generates the desired products. High yields of 79% and 92% were obtained for 3a and 3b, respectively. By increasing the size of the central ring from cyclopentanone to cyclohexanone, the yields decreased to 45% and 40% for 3d and 3e, respectively. Reduced yield may derive from a steric hindrance effect of cyclohexanone, which is obstructive for the nucleophilic addition reaction. The yield for 3c is much lower than that of its methyl-substituted analogue 3b. One reason may be the stronger electron-donating ability of the butyl group, which reduces the electrophilic activity of the aldehyde group. Another possibility is the equilibrium shift of the coupling reaction due to the better solubility of 3c.

Unlike classical Wittig or HWE reactions, which usually generate *cis*- and *trans*-isomer mixtures, exclusively all-*trans* products were obtained in the aldol condensation reactions. The *trans*-configurations were confirmed by ¹H NMR where the proton signals for the CH= group in cycloketone compounds appear at 7.50–7.77 ppm. The chemical shifts of *E*-isomers are usually higher than 7.2 ppm, while the characteristic peaks for the *Z*-isomers appear at ~6.8 ppm. A coupling constant of 15.72 Hz for double bond protons was found, which is typical for the *trans*-isomers in the case of 3a.

Quantum-Chemical Considerations. The optimized most stable structures and electron distributions of the occupied and unoccupied molecular orbitals involved in the population of the lowest excited states of the new TPA PIs and the reference compounds R1 and B3FL are shown in the Supporting Information (Figures S1–S6). The detailed structures and MOs of all studied TPA PIs are also given.

The analysis of the population of the reactive excited triplet state T₁ is shown for the cases of 3a in Figure 2 and 3e in Figure S8. After two-photon absorption ($2 \times 800 \text{ nm} = 2 \times$

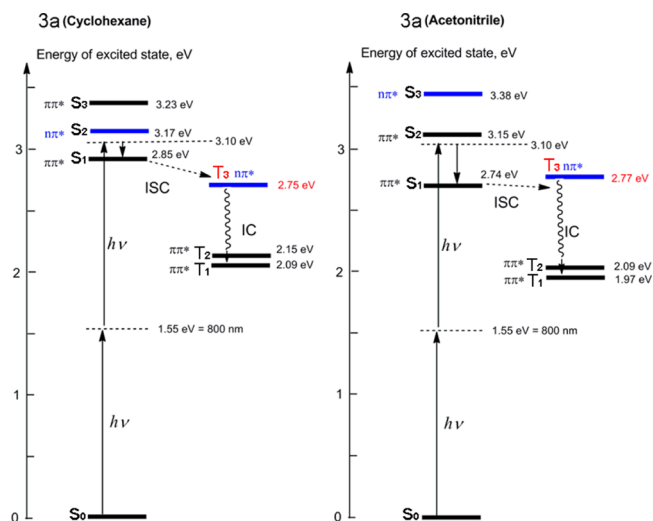


Figure 2. Jablonski energy scheme of the population of the reactive triplet by two-photon excitation of 3a depending on the solvent polarity (calculated at the TDB3LYP/6-31G(d)/SCI-PCM level).

1.55 eV = 3.10 eV), the first excited singlet state S₁ will be populated. The probability of intersystem crossing (ISC) is particularly large for molecules with a second and third triplet state T₂ and T₃ below the S₁ level. Then, the radiationless transition S₁–T₁ can take place either by direct spin–orbital coupling of S₁ to the higher vibrational level of T₁ or by spin–orbital coupling to one of the higher T_n states followed by rapid internal conversion (IC) T_n–T₁, where the efficiency of ISC depends on the extent of the spin–orbital coupling as well as the energy gap between the states involved. This seems to be the case for 3e, where the second and third triplet states lie below, but close to the S₁ state. However, the quantum-chemical calculations showed that the S₁ and both T₁ and T₂ electronic states of 3e are mostly formed by the excitation of electrons from the two highest occupied π -MO's to the two lowest π^* -MO's. But, according to the selection criteria for ISC known as El-Sayed rules,^{52,53} transitions that have the same symmetry (such as S₁(π, π^*) to T₁(π, π^*) or to T₂(π, π^*)) are forbidden. In contrast, the transition from S₁(π, π^*) to T₃(n, π^*), which is formed by excitation of the *n*-electron from HOMO-2, is allowed.

The calculations show that the first excited state S₁ is formed mostly by HOMO–LUMO π -electron excitation in the case of all studied TPA PIs. The results of the calculations are summarized in Table 1. The MOs of all studied TPA PIs are given in the Supporting Information (Figures S1–S6).

The calculations of excitation energies for 3a in different solvents (given in Table 1) show a systematic red shift of the S₁ energy with dependence on the solvent polarity. The calculated red shift between cyclohexane and acetonitrile is about 900 cm⁻¹, which is in good agreement with the experimentally obtained 1500 cm⁻¹ (data not shown). The analysis of the calculated energy scheme for two cases of a nonpolar (cyclohexane) and a polar (acetonitrile) solvent is shown in Figure 2. As can be seen, the excited singlet states S₂ and S₃, which have different symmetry, interchange their position. The triplet state T₃, which has $n\pi^*$ symmetry, has an energy below the excited S₁ state in nonpolar cyclohexane and above it in polar acetonitrile. This gives a good indication for the observed emission quantum yields as a function of solvent polarity.

Table 1. Calculated Energies E (eV) of the Excited States and Oscillator Strengths f

TPA PI	singlet	E (eV)	f		triplet	E (eV)	
R1	S_3	3.59	0.044	$\pi-\pi^*$	T_1	1.77 ^a	$\pi-\pi^*$
	S_2	3.27	0.0001	$\pi-\pi^*$			
	S_1	2.79	2.729	$\pi-\pi^*$			
B3FL	S_4	3.19	0.0002	$n-\pi^*$	T_1	1.47 ^a	$\pi-\pi^*$
	S_3	3.04	2.164	$\pi-\pi^*$			
	S_2	2.54	0.009	$\pi-\pi^*$			
	S_1	2.17	0.437	$\pi-\pi^*$			
3a vacuum	S_3	3.35	0.066	$\pi-\pi^*$	T_3	2.68	$n-\pi^*$
	S_2	3.10	0.0001	$n-\pi^*$	T_2	2.17	$\pi-\pi^*$
	S_1	2.98	1.693	$\pi-\pi^*$	T_1	2.15 (2.02 ^a)	$\pi-\pi^*$
3a cyclohexane	S_3	3.23	0.061	$\pi-\pi^*$	T_3	2.75	$n-\pi^*$
	S_2	3.17	0.0002	$n-\pi^*$	T_2	2.15	$\pi-\pi^*$
	S_1	2.85	1.756	$\pi-\pi^*$	T_1	2.09 (2.02 ^a)	$\pi-\pi^*$
3a acetonitrile	S_3	3.38	0.0000	$n-\pi^*$	T_3	2.77	$n-\pi^*$
	S_2	3.15	0.051	$\pi-\pi^*$	T_2	2.09	$\pi-\pi^*$
	S_1	2.74	2.053	$\pi-\pi^*$	T_1	1.97 (1.84 ^a)	$\pi-\pi^*$
3a water	S_3	3.41	0.0000	$n-\pi^*$	T_3	2.86	$n-\pi^*$
	S_2	3.14	0.048	$\pi-\pi^*$	T_2	2.08	$\pi-\pi^*$
	S_1	2.73	2.104	$\pi-\pi^*$	T_1	1.97 (1.85 ^a)	$\pi-\pi^*$
3b	S_3	3.39	0.062	$\pi-\pi^*$	T_3	2.71	$n-\pi^*$
	S_2	3.05	0.009	$n-\pi^*$	T_2	2.20	$\pi-\pi^*$
	S_1	3.03	2.029	$\pi-\pi^*$	T_1	2.06 (1.95 ^a)	$\pi-\pi^*$
3c	S_3	3.41	0.044	$\pi-\pi^*$	T_1	1.96 ^a	$\pi-\pi^*$
	S_2	3.10	0.032	$n-\pi^*$			
	S_1	2.99	1.839	$\pi-\pi^*$			
3d	S_3	3.35	0.011	$\pi-\pi^*$	T_3	2.75	$n-\pi^*$
	S_2	3.16	0.150	$n-\pi^*$	T_2	2.19	$\pi-\pi^*$
	S_1	2.99	1.455	$\pi-\pi^*$	T_1	2.16 (1.94 ^a)	$\pi-\pi^*$
3e	S_3	3.36	0.013	$\pi-\pi^*$	T_3	2.75	$n-\pi^*$
	S_2	3.16	0.135	$n-\pi^*$	T_2	2.19	$\pi-\pi^*$
	S_1	2.99	1.457	$\pi-\pi^*$	T_1	2.17 (1.95 ^a)	$\pi-\pi^*$

^aEnergy of T_1 calculated as difference of the electronic energies between optimized singlet and triplet states.

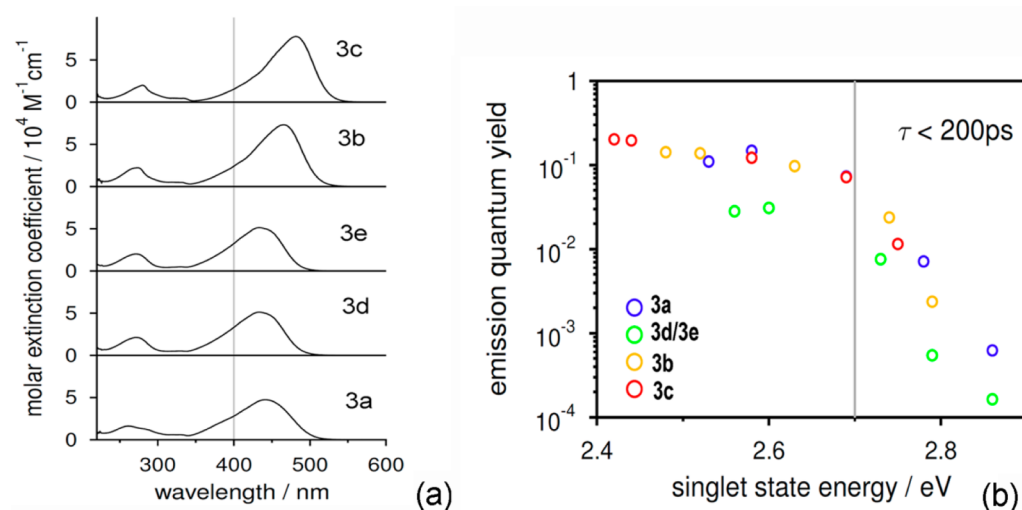


Figure 3. (a) Absorption spectra of the five photoinitiators measured in dichloromethane. Note that the spectra of 3d and 3e are identical. (b) Emission quantum yield as a function of the experimentally determined singlet state energy, E_{00} , calculated according to $(\nu_a^{\max} + \nu_i^{\text{sg}})/2$. The vertical line indicates both fluorescence lifetimes below 200 ps (the time resolution of our setup) and the approximate position of the $n\pi^*$ triplet (Table 1).

One-Photon Optical Spectroscopy. Figure 3a depicts the absorption spectra of photoinitiators 3a to 3e in dichloromethane. All of them exhibit a rather intense ($\epsilon > 5 \times 10^4 \text{ M}^{-1} \text{ cm}^{-1}$) and broad absorption band with the position of the maximum ranging from 430 (3d, 3e) up to 480 nm (3c). In

addition a weaker band (with ϵ around $2 \times 10^4 \text{ M}^{-1} \text{ cm}^{-1}$) is found at 260–270 nm. An even weaker band can be tentatively identified in the region of 320 nm.

Excitation anisotropy of the PIs in dichloromethane in Figure 4 reveals that the lowest energy absorption band is actually

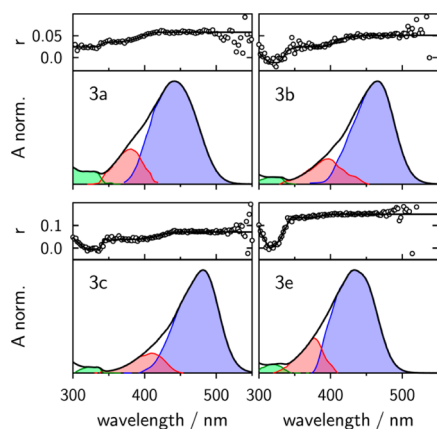


Figure 4. Absorption and excitation anisotropy spectra of PIs 3a to 3e. The solid lines in the anisotropy plot denote the anisotropy dependence used to decompose the absorption spectra.

composed of at least two different electronic transitions.⁵⁴ The low-intensity $n-\pi^*$ transition, predicted from QM calculations for all PIs to also fall into this region, cannot be observed as its oscillator strength is too small (Table 1). However, the predicted energy difference of ~ 0.4 eV between the lowest two $\pi\pi^*$ transitions is well reproduced in our experiments.

The findings of Figures 3 and 4 as well as the data given in Table 2 can be summarized as follows: In line with recent

Table 2. Two-Photon Cross Section, σ_{TPA} , and Maximum Molar Extinction Coefficients, ϵ_{max} ($\pm 10\%$), of the Investigated Initiators in Dichloromethane for the Lowest Energy Absorption Maximum (at λ_{max})

substance	λ_{max} (nm)	$\epsilon_{\text{max}}/10^3$ ($\text{M}^{-1}\text{cm}^{-1}$)	$f(S_1)^a$	λ_{calc}^b (nm)	f^b	$\sigma_{\text{TPA}}^c/\text{GM}$
3a	441	47	0.61	447	1.98	349/269 ^d
3b	466	71	0.78	453	2.02	466
3c	481	78	0.69	460	2.20	327
3d	432	51	0.54	444	1.83	352
3e	432	51	0.54	445	1.80	191

^a $f(S_1)$ denotes the oscillator strength for the S_0-S_1 transition obtained from the absorption spectra using eq 2. ^b λ_{calc} and f denote the calculated absorption maximum of S_1 and its oscillator strength respectively, as calculated in dichloromethane ($\epsilon = 8.93$) (B3LYP/6-31+G(d)/PBF). ^c1 GM = 10^{-50} m⁴ s photon⁻¹; for comparison, Rhodamine B and B3FL were also measured with σ_{TPA} of 114 GM (in MeOH) and 440 GM (in THF), respectively. ^dMeasured in THF.

results by Zhao, Perry, Wu, and co-workers⁵⁵ on a slightly different set of bis(arylidene)cycloalkanones, the energy of the lowest energy absorption band depends as follows on the type of the central acceptor group: cyclohexyl (3d,e) > linear (3a) > cyclopentyl (3b,c). Our quantum-chemical calculations reproduce this trend in dichloromethane exceptionally well (Table 2 and Figure S9). Replacing the amino methyl groups by butyl groups leads to a significant additional bathochromic shift of the absorption maximum.

The maximum molar extinction coefficient, ϵ_{max} , of the lowest energy transition as well the oscillator strength f show a similar trend. The latter is calculated according to⁵⁶

$$f = 4.319 \times 10^{-9} \int \epsilon(\tilde{\nu}) d\tilde{\nu} \quad (2)$$

where the integral has been taken over the lowest energy absorption band, after decomposition of the absorption spectra (Figure 4). ϵ_{max} and f are significantly larger (by 30–50%) for the two PIs with the cyclopentanone ring (3b,c) than for the other 3 PIs, which have all comparable ϵ_{max} and f . It is interesting to note that methyl substitution in the para position to the keto group on the central cyclohexanone ring was found not to affect the one-photon photophysics (band shapes, quantum yields, lifetimes) of the molecule. In fact, all measured photophysical properties for 3d and 3e are identical.

The fluorescence quantum yields are strongly solvent dependent (Figure 3b). Upon increasing the solvent polarity and thus decreasing the S_1-S_0 energy gap, E_{00} , the quantum yield of all PIs strongly increases until reaching an almost constant plateau value. Unfortunately, the time resolution of the used TCSPC does not allow extraction of reasonable radiative and nonradiative rate constants for the interesting range of low emission quantum yields. However, the findings of Table 2 and Figure 5 can be given a simple and convincing

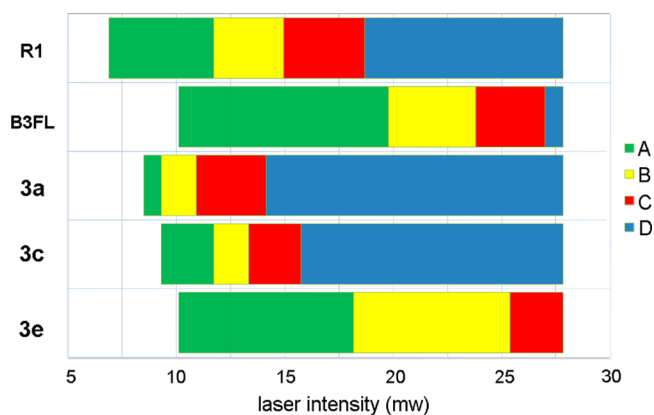


Figure 5. TPIP screening tests (PI concentration: 6.3×10^{-6} mol PI/g resin; writing speed: 50 $\mu\text{m/s}$).

explanation taking into account the quantum-mechanical (QM) calculations. The S_1 state in all PIs can be identified as a $\pi\pi^*$ state. The existence of a closely situated excited $n\pi^*$ triplet state (located at ~ 2.7 eV) makes intersystem crossing—according to the El-Sayed rules—a feasible pathway for deactivation. Upon increasing the solvent polarity, the $\pi\pi^*$ singlet state shifts bathochromically with the $n\pi^*$ triplet state remaining or shifting hypsochromically, thus increasing the energy gap between these two states. As a result, the intersystem crossing contribution to the nonradiative deactivation channel is reduced and the emission quantum yields increase. These observations are in striking contrast to the behavior of reference R1 and B3FL. R1 shows an almost solvent independent high emission quantum yield in the range from 0.59 to 0.79 in cyclohexane and acetonitrile, respectively.¹³ B3FL, on the other hand, shows the opposite solvent dependence for emission quantum yield. Here, Φ_f decreases upon increasing the solvent polarity. In contrast to the participation of the triplet state as for the PIs investigated here, this behavior has been attributed to the population of a strongly polar (charge transfer) excited state, the charge recombination of which—back to the ground state—seems to be governed by the free energy gap law.³³ For the PIs studied here the initiation efficiency will thus be strongly dependent, among many other factors such as radical production efficiency, radical survival probability, etc., not only

on the two-photon absorption cross section but equally well if not more importantly by the feasibility of undergoing intersystem crossing to the active triplet state.

Table 3. Emission Properties of 3a–e in Five Different Solvents^a

solvent	DK	<i>n</i>	<i>E</i> ₀₀ (eV)	Φ _f	τ _f (ns)
3a					
cyclohexane	2.0	1.4235	2.86	6.2 × 10 ⁻⁴	
<i>n</i> -butyl ether	3.1	1.3968	2.78	7.1 × 10 ⁻³	
<i>n</i> -propyl acetate	6.0	1.3828	2.69	7.3 × 10 ⁻²	0.20
dichloromethane	8.9	1.4210	2.58	1.5 × 10 ⁻¹	0.58
acetonitrile	35.9	1.3410	2.53	1.1 × 10 ⁻¹	0.76
3b					
cyclohexane	2.0	1.4235	2.79	2.4 × 10 ⁻³	
<i>n</i> -butyl ether	3.1	1.3968	2.74	2.4 × 10 ⁻²	
<i>n</i> -propyl acetate	6.0	1.3828	2.63	9.7 × 10 ⁻²	0.56
dichloromethane	8.9	1.4210	2.52	1.4 × 10 ⁻¹	0.59
acetonitrile	35.9	1.3410	2.48	1.4 × 10 ⁻¹	0.68
3c					
cyclohexane	2.0	1.4235	2.75	1.2 × 10 ⁻²	0.35
<i>n</i> -butyl ether	3.1	1.3968	2.69	7.2 × 10 ⁻²	0.37
<i>n</i> -propyl acetate	6.0	1.3828	2.58	1.2 × 10 ⁻¹	0.46
dichloromethane	8.9	1.4210	2.44	2.0 × 10 ⁻¹	0.72
acetonitrile	35.9	1.3410	2.42	2.0 × 10 ⁻¹	0.80
3d/3e					
cyclohexane	2.0	1.4235	2.86	1.6 × 10 ⁻⁴	
<i>n</i> -butyl ether	3.1	1.3968	2.79	5.5 × 10 ⁻⁴	
<i>n</i> -propyl acetate	6.0	1.3828	2.73	4.6 × 10 ⁻³	
dichloromethane	8.9	1.4210	2.60	9.5 × 10 ⁻³	
acetonitrile	35.9	1.3410	2.56	2.2 × 10 ⁻²	0.2

^a*E*₀₀ is the 0–0 transition energy calculated as (ν_a^{max} + ν_f^{cg})/2, where ν_a^{max} is the absorption maximum of the lowest energy absorption band and ν_f^{cg} is the center of gravity of the emission band (both in transition dipole moment representation).⁵⁷ Φ_f is the fluorescence quantum yield and τ_f the fluorescence lifetime. DK and *n* are the dielectric constant and refractive index of the solvent at 25 °C, respectively, from ref 58.

Two-Photon Absorption Cross Section. To investigate the TPA properties of the new PIs, an open aperture *z*-scan analysis was performed to determine the TPA cross sections at 800 nm. Chloroform was used as solvent for the TPA characterization of all new PIs. The experimental data of 3e are provided as a representative example and were fitted using the adopted equations of Sheik-Bahae et al.⁵⁹ to obtain the σ_{TPA}. To exclude excited-state absorption and to verify that a pure σ_{TPA} is determined, the measurements were repeated at different peak intensities and the calculated parameter *q*₀ scales linearly with intensity (Figure S10). All calculated σ_{TPA} values are given in Table 2.

The cross-section value of the reference compound Rhodamine B is in good agreement with our previous result and the literature, verifying the reliability of the experimental setup. Since intramolecular charge transfer is utilized as the “driving force” for TPA, strong electron-donor and electron-acceptor groups are required. In addition, long π-conjugated bridges and good coplanarity, which lead to states with extended charge separation, are critical in enhancing the efficiency of intramolecular charge transfer. The investigated benzylidene ketone-based TPA PIs comprise typical D-π-A-π-D core structures with C_{2v} symmetry, where dialkylamino groups act as donors, vinyl

as π-conjugated bridges, and carbonyl as acceptors. The open chain acetone-based PI 3a exhibits a large σ_{TPA} of 349 GM. When changing the acceptor group in 3a from an acetone group to a cyclopentanone moiety as in 3b, the value even increased to 466 GM. The enhancement may be due to a relatively higher molecular rigidity as well as a higher degree of conjugation compared to 3a.⁶⁰ Substitution of the *N*-methyl groups by butyl groups as in 3c led to a reduced σ_{TPA} of 327 GM. An explanation can be given by the red-shift-induced low TPA absorption at the given wavelength. Another reason, as indicated in quantum-chemical calculations, is the deformation of the central cyclopentanone ring in 3c due to the strong distortion induced by the large NBU₂ group. The nonplanar nature of the ring could decrease the conjugation and therefore lead to weak TPA.

When increasing the size of the central ketone from cyclopentanone to cyclohexanone as in 3d, the σ_{TPA} value dropped to 352 GM. The reduction in TPA absorption might be explained by the nonplanarity of the six-membered ring, which leads to a decrease in the degree of conjugation. Interestingly, although the linear absorption spectrum of 3d is identical to that of 3e, methyl substitution at the 4-position on cyclohexanone dramatically reduced the σ_{TPA} of 3e to 191 GM. The above results indicate that not only the size of the central ring but also the ring substitution could significantly affect the TPA behavior of the benzylidene ketone-based initiators.

As only the absorption behavior could be obtained via *z*-scan measurement, TPIP structuring tests were performed to further characterize the TPA initiation efficiency of the new PIs.

TPIP Structuring Test. There are several methods to estimate the initiation efficiency of initiators in TPIP, such as single-line writing, in which the resolution is the most important parameter.⁶¹ Here, we use more complicated 3D shapes fabricated under various laser intensities and writing speeds for the evaluation. Such a method is more practical since broad ideal processing windows are critical for high throughput in mass production and for some specific applications like waveguide fabrication for printed circuit boards.³ Defined woodpile structures (lateral dimension: 50 × 50 μm, 5 μm hatch distance, 0.7 μm layer distance, 20 layers) were written into the monomer formulation by means of TPIP to evaluate the activity of the PIs. The laser intensity was screened in a range of 1–27.82 mW (measured after passing the 100× microscope objective). A 1:1 mixture of trimethylolpropane triacrylate (TTA) and ethoxylated (20/3) trimethylolpropane triacrylate (ETA) as an acrylate-based test resin with the same molar PI concentration of 6.3 × 10⁻⁶ mol PI/g resin (0.2 wt % of 3e) was used, since good results had been previously obtained for such a formulation.

The different color of the bars and their corresponding classes in Figure 5 were used to evaluate the TPA initiation efficiency of the initiators at a writing speed of 50 μm/s (full processing windows of all initiators at different laser intensities and feed rates shown in Figure S11). Four classes were employed to indicate the quality of the structures (Figure 6a). Class A defines excellent structures with fine hatch lines (the line width is about 400 nm) and class B good structures with thick hatch lines (compared to class A) or slightly contorted structures. Generally, broader ideal processing windows (class A and B) and lower laser intensities are desired for high throughput in mass production. Structures rated as class C have identified shapes but with small mistakes (e.g., holes, burst regions caused by overexposure). Parts structured with laser

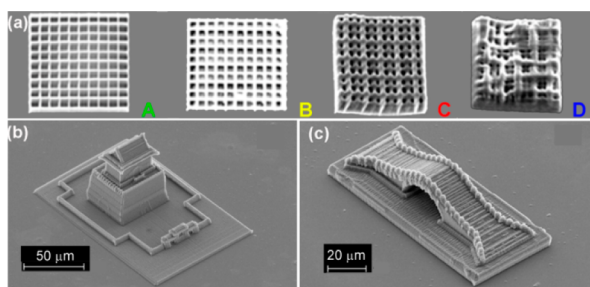


Figure 6. (a) Classification of the structures by the typical quality of their shapes. (b) Ancient tower in oriental style. (c) Chinese Jade Belt Bridge.

intensities rated as class D no longer showed acceptable results. The shapes are no longer identifiable, showing completely missing walls and/or vast holes.

In our measurements, the well-known initiator from the literature **R1** can be used to build nicely shaped structures at low laser intensities. On the other hand, the 2-,7-substituted fluorenone-based PI **B3FL** exhibits excellent performance in the TPIP test. Although a slightly higher laser intensity is required for **B3FL** compared to **R1**, the ideal processing windows of **B3FL** are much broader than that of **R1**. The higher efficiency of such a triple-bond-containing PI may derive from the larger σ_{TPA} , the exclusion of photoinduced *cis*–*trans* isomerization, and the lower fluorescence quantum yield.

The acetone-based initiator **3a** gives nice structures at lower laser intensity than **B3FL**, but its ideal processing windows are significantly smaller. One reason is the relatively smaller TPA cross section of **3a**. Another main reason for the low efficiency of **3a** lies in its strong fluorescence emission, which deactivates the active triplet state. In addition, the photochemical *cis*–*trans* isomerization deactivation processes could reduce the initiation efficiency as well. By changing the acceptor group in **3a** from an acetone group to a cyclopentanone moiety as in **3b**, the solubility in the resins was dramatically decreased. An attempt to improve its solubility by adding drops of various organic solvents finally failed because of the heterogeneous solution obtained. Therefore, we were not able to get any comparable result with **3b** in the structuring tests due to its poor solubility (data not shown). The substitution of the *N*-methyl groups by butyl groups in the cyclopentanone-based initiator **3c** resolved the solubility problem. The ideal processing windows of **3c** are slightly broader than those of **3a**. The improvement may derive from the rigidity of the ring, which confines the rotation of the double bonds and thus reduces isomerization deactivation.

When increasing the size of the central ketone from cyclopentanone to cyclohexanone as in **3d**, the solubility improved to some extent due to its nonplanar molecular structure. The PI readily dissolved in the resin with the assistance of a few drops of chloroform. However, some precipitate formed when removing the last traces of solvent at 40 °C under vacuum. Therefore, similar to **3b**, no comparable result for **3d** could be obtained (data not shown). By changing the electron acceptor from cyclohexanone to 4-methylcyclohexanone as in **3e**, the solubility significantly improved. The enhancement is attributed to increased steric hindrance, which facilitates the dispersion of PI in the resin. Surprisingly, although **3e** exhibits the smallest σ_{TPA} among the investigated PIs, the ideal processing windows are much broader than those of other benzylidene ketone PIs and reference PI **R1**. The initiation efficiency is dependent not only on σ_{TPA} but also on

the quantum yields of active radical formation. Although initiator **3e** possesses the smallest σ_{TPA} , its fluorescence quantum yield is 5–10 times smaller than that of its analogues. Low fluorescence quantum yields are essential for efficient photoinitiators as this leads to less radiative deactivation and a higher population of the active state for initiating the polymerization. Such considerable enhancement was also observed by Duan's group^{62,63} while studying the photoinitiation efficiency of other similar C_{2v} , symmetrical TPA PIs. For initiator **3e**, high radical formation quantum yields tend to compensate its low TPA cross section to ensure high initiation efficiency. The kind of compensation is common for some traditional UV photoinitiators, such as Irgure 369⁶⁴ and Lucirin TPO-L,⁶⁵ which are still used in TPIP. The activity of **3e** in TPIP tests is as high as that of **B3FL**. It should be mentioned that **3e** could be simply prepared in one step while the synthesis of **B3FL** required four steps and involved an expensive palladium catalyst. In contrast to **R1**, which induces polymerization under UV irradiation, **3e** is surprisingly stable under one-photon conditions, and nearly no photoinitiation activity was found in classical photo differential scanning calorimetry (photo-DSC) experiment. Furthermore, the normal DSC result showed that the formulation with **3e** as initiator was stable below 170 °C in the absence of light (temperature range between 50 and 200 °C at a heating rate of 10 °C min⁻¹).

Additionally, more complex 3D structures (Figure 6b,c) were inscribed into the material volume with an acrylate-based formulation containing **3e** (0.2 wt %) as initiator. Delicate 3D models with high spatial resolution, which is otherwise inaccessible for other rapid prototyping techniques, can be easily obtained.

With the same formulation, only 4 min is required for fabricating a 3D racing car model, which is of 285 × 130 × 50 μm³ in dimensions and consisted of 100 layers at an average of 200 polymer lines each (Supporting Information). Taking the time used for positioning the mechanics, the focal point was traced in the resin at well above 80 mm/s. Because of inertia limitations of the experimental setup, the scanning speed is limited for this specific CAD structure. Our recent study showed that using **3e** as initiator, a 300 μm wide cube, sliced into layers of equidistant polymer lines, can be fabricated even within methacrylate-based formulations at the speed of several m/s (detailed information will be published in the future). This is remarkable since previously reported scanning speeds are below 10 mm/s.⁶⁶

CONCLUSION

A series of benzylidene ketone-based two-photon initiators containing dialkylamino groups as donors and double bonds as conjugation bridges were simply synthesized via classical aldol condensation reactions. The systematic evaluation of structure–property relationships via quantum-chemical calculations combined with experimental tests confirmed the significant central ring effects on the photophysical and photochemical properties. Although the fluorescence lifetimes and quantum yields of all investigated initiators were strongly solvent-dependent, the cyclohexanone-based initiators **3d** and **3e** showed much weaker fluorescence emission and shorter fluorescence lifetime than their cyclopentanone counterparts, **3b** and **3c**. With good coplanarity and a suitably strong absorption at the desired wavelength, **3b** possessed the largest σ_{TPA} of 466 GM at 800 nm in the *z*-scan measurement, while **3d** and **3e** exhibited reduced σ_{TPA} due to the nonplanarity of

the six-membered rings, which leads to a decreasing degree of conjugation. Surprisingly, **3e**, with the smallest σ_{TPA} among the investigated initiators, displayed much broader ideal processing windows than other benzylidene ketone PIs and the reference PI **R1** in TPIP tests. The activity of **3e** in TPIP tests is as high as that of **B3FL**, but the preparation of **3e** is much simpler and more economical. A writing speed as high as 80 mm/s was obtained for microfabrication of complex 3D structures with acrylate-based formulations containing **3e** as photoinitiator. The straightforward synthetic routine combined with high TPA initiation efficiency as well as excellent thermal and one-photon stability of these TPA initiators shows great potential for commercialization.

■ ASSOCIATED CONTENT

■ Supporting Information

Quantum-chemical calculations, z-scan measurement for TPA cross section, processing windows of TPA PIs, and video of microfabrication of racing car. This material is available free of charge via the Internet at <http://pubs.acs.org>.

■ AUTHOR INFORMATION

Corresponding Author

*E-mail robert.liska@tuwien.ac.at.

Notes

The authors declare no competing financial interest.

■ ACKNOWLEDGMENTS

The authors acknowledge the financial support by the China Scholarship Council (CSC, no. 2009688004), Swiss SNF project 200020-124393, Austrian Science Fund (FWF; N703 ISOTEC), the Austrian Research Agency (FFG 819718), and European Science Foundation (ESF) with P2M network.

■ REFERENCES

- (1) Serbin, J.; Gu, M. *Adv. Mater.* **2006**, *18*, 221–224.
- (2) Sun, H.-B.; Matsuo, S.; Misawa, H. *Appl. Phys. Lett.* **1999**, *74*, 786–788.
- (3) Krivec, S.; Matsko, N.; Satzinger, V.; Pucher, N.; Galler, N.; Koch, T.; Schmidt, V.; Grogger, W.; Liska, R.; Lichtenegger, H. C. *Adv. Funct. Mater.* **2010**, *20*, 811–819.
- (4) Parthenopoulos, D. A.; Rentzepis, P. M. *Science* **1989**, *245*, 843–845.
- (5) Pudavar, H. E.; Joshi, M. P.; Prasad, P. N.; Reinhardt, B. A. *Appl. Phys. Lett.* **1999**, *74*, 1338–1340.
- (6) Maruo, S.; Nakamura, O.; Kawata, S. *Opt. Lett.* **1997**, *22*, 132–134.
- (7) Malval, J.-P.; Jin, M.; Morlet-Savary, F.; Chaumeil, H. I. n.; Defoin, A.; Soppera, O.; Scheul, T.; Bouriau, M.; Baldeck, P. L. *Chem. Mater.* **2011**, *23*, 3411–3420.
- (8) Belfield, K. D.; Ren, X.; Hagan, E. W.; Stryland, E. W.; Hagan, D. J.; Dubikovskiy, V.; Miesak, E. J. *J. Am. Chem. Soc.* **2000**, *122*, 1217–1218.
- (9) Belfield, K. D.; Schafer, K. J.; Liu, Y.; Liu, J.; Ren, X.; Stryland, E. W. V. *J. Phys. Org. Chem.* **2000**, *13*, 837–849.
- (10) Schafer, K. J.; Hales, J. M.; Balu, M.; Belfield, K. D.; Van Stryland, E. W.; Hagan, D. J. *J. Photochem. Photobiol., A* **2004**, *162*, 497–502.
- (11) Wang, X.; Jin, F.; Chen, Z.; Liu, S.; Wang, X.; Duan, X.; Tao, X.; Jiang, M. *J. Phys. Chem. C* **2011**, *115*, 776–784.
- (12) Cumpston, B. H.; Ananthavel, S. P.; Barlow, S.; Dyer, D. L.; Ehrlich, J. E.; Erskine, L. L.; Heikal, A. A.; Kuebler, S. M.; Lee, I. Y. S.; McCord-Maughon, D.; Qin, J.; ckel, H.; Rumi, M.; Wu, X.-L.; Marder, S. R.; Perry, J. W. *Nature* **1999**, *398*, 51–54.
- (13) Pucher, N.; Rosspeintner, A.; Satzinger, V.; Schmidt, V.; Gescheidt, G.; Stampfl, J.; Liska, R. *Macromolecules* **2009**, *42*, 6519–6528.
- (14) Li, C.; Luo, L.; Wang, S.; Huang, W.; Gong, Q.; Yang, Y.; Feng, S. *Chem. Phys. Lett.* **2001**, *340*, 444–448.
- (15) He, G. S.; Tan, L.-S.; Zheng, Q.; Prasad, P. N. *Chem. Rev.* **2008**, *108*, 1245–1330.
- (16) Yagci, Y.; Jockusch, S.; Turro, N. J. *Macromolecules* **2010**, *43*, 6245–6260.
- (17) Tian, Y.; Zhang, M.; Yu, X.; Xu, G.; Ren, Y.; Yang, J.; Wu, J.; Zhang, X.; Tao, X.; Zhang, S.; Jiang, M. *Chem. Phys. Lett.* **2004**, *388*, 325–329.
- (18) Lemerrier, G.; Martineau, C. c.; Mulatier, J.-C.; Wang, I. n.; Stéphane, O.; Baldeck, P.; Andraud, C. *New J. Chem.* **2006**, *30*, 1606–1613.
- (19) Porshnev, Y. N.; Churkina, V. A.; Titov, V. V. *Chem. Heterocycl. Compd.* **1978**, *14*, 1070–1074.
- (20) Lin, T.-C.; Hsu, C.-S.; Hu, C.-L.; Chen, Y.-F.; Huang, W.-J. *Tetrahedron Lett.* **2009**, *50*, 182–185.
- (21) Beletskaya, I. P.; Cheprakov, A. V. *Chem. Rev.* **2000**, *100*, 3009–3066.
- (22) Malval, J.-P.; Morlet-Savary, F.; Chaumeil, H.; Balan, L.; Versace, D.-L.; Jin, M.; Defoin, A. *J. Phys. Chem. C* **2009**, *113*, 20812–20821.
- (23) Chinchilla, R.; Nájera, C. *Chem. Rev.* **2007**, *107*, 874–922.
- (24) Huang, X.; Shi, Q.; Chen, W.-Q.; Zhu, C.; Zhou, W.; Zhao, Z.; Duan, X.-M.; Zhan, X. *Macromolecules* **2010**, *43*, 9620–9626.
- (25) Monroe, B. M.; Smothers, W. K.; Keys, D. E.; Krebs, R. R.; Mickish, D. J.; Harrington, A. F.; Schicker, S. R.; Armstrong, M. K.; Chan, D. M. T.; Weathers, C. I. *J. Imaging Sci.* **1991**, *35*, 19–25.
- (26) Wu, J.; Zhao, Y.; Li, X.; Shi, M.; Wu, F.; Fang, X. *New J. Chem.* **2006**, *30*, 1098–1103.
- (27) Xue, J.; Zhao, Y.; Wu, J.; Wu, F. *J. Photochem. Photobiol., A* **2008**, *195*, 261–266.
- (28) Xue, J.; Zhao, Y.; Wu, F.; Fang, D.-C. *J. Phys. Chem. A* **2010**, *114*, 5171–5179.
- (29) Sarkisov, S. S.; Peterson, B. H.; Curley, M. J.; Nesterov, V. N.; Timofeeva, T.; Antipin, M.; Radovanova, E. I.; Leyderman, A.; Fleitz, P. A. *J. Nonlinear Opt. Phys.* **2005**, *14*, 21–40.
- (30) Wang, P.; Du, W.; Wu, S. *Huaxue Xuebao* **1992**, *50*, 1140–1144.
- (31) Yamashita, K.; Imahashi, S.; Ito, S. *Dyes Pigm.* **2008**, *76*, 748–753.
- (32) Xing, J.-F.; Chen, W.-Q.; Dong, X.-Z.; Tanaka, T.; Fang, X.-Y.; Duan, X.-M.; Kawata, S. *J. Photochem. Photobiol., A* **2007**, *189*, 398–404.
- (33) Li, Z.; Siklos, M.; Pucher, N.; Cicha, K.; Ajami, A.; Husinsky, W.; Rosspeintner, A.; Vauthey, E.; Gescheidt, G.; Stampfl, J.; Liska, R. *J. Polym. Sci., Polym. Chem.* **2011**, *49*, 3688–3699.
- (34) Olomucki, M.; Le Gall, J. Y. *Bull. Soc. Chim. Fr.* **1976**, *9–10* (Pt. 2), 1467–1468.
- (35) Doroshenko, A. O.; Grigorovich, A. V.; Posokhov, E. A.; Pivovarenko, V. G.; Demchenko, A. P.; Sheiko, A. D. *Russ. Chem. B* **2001**, *50*, 404–412.
- (36) Rao, C. B.; Raju, P. V. N. *Indian J. Chem. B* **1984**, *23*, 321–327.
- (37) Wallach. *Chem. Zentralbl.* **1908**, *79*, 639.
- (38) Becke, A. D. *J. Chem. Phys.* **1993**, *98*, 5648–5652.
- (39) Becke, A. D. *J. Chem. Phys.* **1996**, *104*, 1040–1046.
- (40) Lee, C. T.; Yang, W. T.; Parr, R. G. *Phys. Rev. B* **1988**, *37*, 785–789.
- (41) Jaguar, version 7.8, Schrodinger LLC, New York, 2010.
- (42) Bauernschmitt, R.; Ahlrichs, R. *Chem. Phys. Lett.* **1996**, *256*, 454–464.
- (43) Gaussian 03, Revision B.02: Frisch, M. J.; Trucks, G. W.; Schlegel, H. B.; Scuseria, G. E.; Robb, M. A.; Cheeseman, J. R.; Montgomery, Jr., J. A.; Vreven, T.; Kudin, K. N.; Burant, J. C.; Millam, J. M.; Iyengar, S. S.; Tomasi, J.; Barone, V.; Mennucci, B.; Cossi, M.; Scalmani, G.; Rega, N.; Petersson, G. A.; Nakatsuji, H.; Hada, M.; Ehara, M.; Toyota, K.; Fukuda, R.; Hasegawa, J.; Ishida, M.; Nakajima, T.; Honda, Y.; Kitao, O.; Nakai, H.; Klene, M.; Li, X.; Knox, J. E.;

Hratchian, H. P.; Cross, J. B.; Bakken, V.; Adamo, C.; Jaramillo, J.; Gomperts, R.; Stratmann, R. E.; Yazyev, O.; Austin, A. J.; Cammi, R.; Pomelli, C.; Ochterski, J. W.; Ayala, P. Y.; Morokuma, K.; Voth, G. A.; Salvador, P.; Dannenberg, J. J.; Zakrzewski, V. G.; Dapprich, S.; Daniels, A. D.; Strain, M. C.; Farkas, O.; Malick, D. K.; Rabuck, A. D.; Raghavachari, K.; Foresman, J. B.; Ortiz, J. V.; Cui, Q.; Baboul, A. G.; Clifford, S.; Cioslowski, J.; Stefanov, B. B.; Liu, G.; Liashenko, A.; Piskorz, P.; Komaromi, I.; Martin, R. L.; Fox, D. J.; Keith, T.; Al-Laham, M. A.; Peng, C. Y.; Nanayakkara, A.; Challacombe, M.; Gill, P. M. W.; Johnson, B.; Chen, W.; Wong, M. W.; Gonzalez, C.; Pople, J. A. Gaussian, Inc., Wallingford, CT, 2004.

(44) Tannor, D. J. M.; Murphy, B.; Friesner, R.; Sitkoff, R. A.; Nicholls, D.; Ringnalda, A.; Goddard, W. A., III; Honig, B. *J. Am. Chem. Soc.* **1994**, *116*, 11875–11882.

(45) Foresman, J. B.; Keith, T. A.; Wiberg, K. B.; Snoonian, J.; Frisch, M. J. *J. Phys. Chem.* **1996**, *100*, 16098–16104.

(46) ChemBio3D Ultra, version 12.0, CambridgeSoft, 1986–2009.

(47) Gardecki, J. A.; Maroncelli, M. *Appl. Spectrosc.* **1998**, *52*, 1179–1189.

(48) Van Gompel, J. A.; Schuster, G. B. *J. Phys. Chem.* **1989**, *93*, 1292–1295.

(49) Valeur, B. *Molecular Fluorescence: Principles and Applications*; Wiley-VCH: Weinheim, 2001; p 161.

(50) An, L. T.; Zou, J. P.; Zhang, L. L. *Catal. Commun.* **2008**, *9*, 349–354.

(51) Watanabe, K.; Imazawa, A. *Bull. Chem. Soc. Jpn.* **1982**, *55*, 3208–3211.

(52) Klessinger, M.; Michl, J. *Lichtabsorption und Photochemie organischer Moleküle*; VCH Verlagsgesellschaft: Weinheim, 1989; p 255.

(53) El-Sayed, M. A. *J. Chem. Phys.* **1963**, *38*, 2834–2838.

(54) Valeur, B.; Weber, G. *Photochem. Photobiol.* **1977**, *25*, 441–444.

(55) Zou, Q.; Zhao, Y.; Makarov, N. S.; Campo, J.; Yuan, H.; Fang, D.-C.; Perry, J. W.; Wu, F. *Phys. Chem. Chem. Phys.* **2012**, *14* (33), 11743–11752.

(56) Birks, J. B. *Photophysics of Aromatic Molecules*; Wiley Monographs in Chemical Physics; Wiley-Interscience: London, 1970; p 51.

(57) Angulo, G.; Grampp, G.; Rosspeintner, A. *Spectrochim. Acta, Part A* **2006**, *65*, 727–731.

(58) Marcus, Y. *The Properties of Solvents*; Wiley Series in Solution Chemistry; John Wiley & Sons Ltd.: Weinheim, 1998; Vol. 4.

(59) Sheik-Bahae, M.; Said, A. A.; Wei, T. H.; Wu, Y. Y.; Hagan, D. J.; Soileau, M. J.; Van Stryland, E. W. *Proc. SPIE* **1990**, *1148*, 41–51.

(60) Yuan, H.; Zhao, Y.; Wu, F. *Chem. Mater.* **2012**, *24*, 1371–1377.

(61) Xing, J.-F.; Dong, X.-Z.; Chen, W.-Q.; Duan, X.-M.; Takeyasu, N.; Tanaka, T.; Kawata, S. *Appl. Phys. Lett.* **2007**, *90*, 131106/1–131106/3.

(62) Xing, J.-F.; Chen, W.-Q.; Gu, J.; Dong, X.-Z.; Takeyasu, N.; Tanaka, T.; Duan, X.-M.; Kawata, S. *J. Mater. Chem.* **2007**, *17*, 1433–1438.

(63) Xing, J.-F.; Zheng, M.-L.; Chen, W.-Q.; Dong, X.-Z.; Takeyasu, N.; Tanaka, T.; Zhao, Z.-S.; Duan, X.-M.; Kawata, S. *Phys. Chem. Chem. Phys.* **2012**, *14*, 15785–15792.

(64) Ovsianikov, A.; Schlie, S.; Ngezhahayo, A.; Haverich, A.; Chichkov, B. N. *J. Tissue Eng. Regener. Med.* **2007**, *1*, 443–449.

(65) Mendonca, C. R.; Correa, D. S.; Baldacchini, T.; Tayalia, P.; Mazur, E. *Appl. Phys. A: Mater. Sci. Process.* **2008**, *90* (4), 633–636.

(66) Farsari, M.; Filippidis, G.; Sambani, K.; Drakakis, T. S.; Fotakis, C. *J. Photochem. Photobiol., A* **2006**, *181*, 132–135.